DIGITALCOMMONS
—@WAYNESTATE—

Wayne State University

Civil and Environmental Engineering Faculty
Research Publications

Civil and Environmental Engineering

3-5-2013

Analysis of Alternative Ductile Fiber-reinforced Polymer Reinforcing Bar Concepts

Bashar Behnam
Broome College, Binghamton, NY

Christopher D. Eamon
Wayne State University, Detroit, MI, christopher.eamon@wayne.edu

Analysis of Alternative Ductile FRP Reinforcing Bar Concepts

Bashar Behnam[1] and Christopher Eamon[2]

ABSTRACT

Steel-reinforced concrete structural components are often associated with significant maintenance costs as a result of reinforcement corrosion. To mitigate this problem, fiber-reinforced polymer (FRP) bars have been used in place of traditional steel reinforcement for some applications. The non-ductile response of typical FRP bars is a concern, however. To overcome this problem, hybrid ductile FRP (HDFRP) bars have been developed for use in concrete flexural members with resulting ductility indices similar to sections reinforced with steel. In this study, five different HDFRP bar concepts are analyzed and compared in terms of ductility, stiffness, and relative cost. Of primary interest is the effect that the number of materials used in bar construction has on performance. Reinforced concrete beam and bridge deck applications are considered for analysis. It was found that all HDFRP-reinforced flexural members considered could meet code-specified strength and ductility requirements for steel-reinforced sections, although service load deflections were approximately twice that of steel-reinforced sections of the same depth. In general, ductility increased, and overall material cost decreased, as the bar material layers increased from 2 to 4. The 4-material continuous fiber bar approach was found to be most promising, with high ductility as well as relatively low cost.

---

[1] Assistant Professor, Dept. of Civil Engineering Technology, Broom College, Binghamton, NY 13905. Email: as2732@wayne.edu.

[2] Associate Professor, Dept. of Civil and Environmental Engineering, Wayne State University. Detroit, MI 48202. Email: eamon@eng.wayne.edu. PH: 313-577-3766

INTRODUCTION

Extensive damage is caused to the civil infrastructure by steel reinforcement corrosion, where in the United States alone, upwards of 30% of bridges have been significantly affected by corrosion-induced deterioration, representing a repair cost of over $8 billion [1,2]. Bridge decks exposed to chlorides are particularly susceptible to this problem, where corroding steel may significantly increase in volume and fracture the concrete around which bars are embedded [3]. To prevent this damage, various approaches have been considered, including using epoxy-coated bars; implementing cathodic protection measures; shielding bars from chloride penetration by increasing cover; and altering concrete properties to limit chloride action; among others. Although some damage mitigation has been achieved with these methods, a substantial corrosion problem still remains [2,3].

A more recent approach to address this problem is to avoid the use of steel altogether, and reinforce concrete members using fiber reinforced polymer (FRP) composite materials. Although relatively small in number, FRP-reinforced concrete components have been implemented throughout the world as well as in the US, where the construction of various structures have been documented in the technical literature [4]. Currently, the two prevailing US guidelines governing reinforced concrete structural design, The American Association of State and Highway Transportation Officials (AASHTO) *Bridge Design Specifications* [5] and the American Concrete Institute *Building Code Requirements for Structural Concrete*, ACI-318 [6], for bridges and buildings, respectively, do not contain detailed guidelines for the use of FRP. However, both ACI as well as AASHTO have alternative design guides available that specifically address the use of FRP reinforcing bars in concrete flexural members: the *ACI Guide for the Design and Construction of Structural Concrete Reinforced with FRP Bars, ACI-440.1R*

[7], as well as the *AASHTO LRFD Bridge Design Guide Specifications for GFRP-Reinforced Concrete Bridge Decks and Traffic Railings* [8].

Despite the availability of these design guides, the number of newly-constructed FRP-reinforced structures, relative to steel-reinforced structures, is very small. Various factors contribute to the limited use of FRP, such as high initial cost, lack of familiarity among designers, low stiffness, and lack of ductility. Poor material and bar geometry choices may also lead to other problems, such as inadequate bond and material degradation, although most of these issues can be solved with careful selection of bar properties [9].

In recent years, two of the major challenges with FRP, high cost and lack of ductility, have been considered by various researchers. Ductility is a particular concern from a safety perspective [10], as the nearly linear-elastic response of traditional FRP bars until rupture allows little warning before failure, nor does it allow moments to be significantly redistributed in indeterminate structures. In the last two decades, however, work has been done by various researchers to increase ductility, and significant ductility has been achieved by numerous bar designs [1, 9-15]. Although different techniques have been proposed to achieve pseudo-ductile response in FRP structures, most successful ductile FRP reinforcement bar designs have use the "hybrid" approach. Here, the bars are manufactured not with a single fiber, but with several fibers that have different ultimate strain values. Under load, the fibers incrementally fail as the strain increases, reducing stiffness but retaining sufficient strength to produce an effective ductile response. When used in concrete flexural members, the hybrid bars have generated moment-curvature responses that are similar to steel-reinforced concrete members [9, 12].

High cost remains an important issue for the use of FRP, as common FRP reinforcing bars may cost up to 8 times more than steel reinforcement. However, the reduced corrosion-

induced maintenance costs generally become beneficial in the long run, where life-cycle cost analyses of FRP-reinforced bridges revealed significant cost savings over a 50 to 75 year bridge lifetime, typically resulting in half or less of the total life-cycle cost of corresponding steel-reinforced bridges. In the considered cases, cost savings usually began at approximately 20 years into the service life of the bridge [4].   However, with an expected 20-year pay-back period, initial cost is still a major concern, and any initial cost savings are clearly highly desirable.

In light of these critical issues for ductile FRP bars, this paper presents an analysis of several hybrid ductile fiber reinforced polymer (HDFRP) reinforcing bar concepts.   The objective of this study is to compare bar performance, in terms of ductility, stiffness, and cost, for different HDFRP bars. Of primary interest in this study is the effect that material choices, particularly in terms of the type and number of materials used in bar construction, have on bar performance.   The effect of other factors related to the manufacturing of some bars, such as braiding, crimping, and twisting of the continuous fibers, are difficult to predict analytically and are not considered in this study.

HDFRP BARS CONSIDERED

Various bar layouts are possible, with a generic scheme shown in Figure 1. In the figure, FRP materials are placed in concentric layers for illustration, although bar construction is not limited to this geometry. Note that a relatively narrow range of bar layouts is actually feasible, once several other practical design constraints are considered, restricting the range of possible material properties and volume fractions, as discussed below.

In this study, five HDFRP bar concepts are considered: 2, 3, and 4-material bars composed of continuous fibers, designated *B1*, *B2*, and *B3*, respectively; a 4-material bar composed of 2 layers of continuous fibers and 2 layers of randomly-dispersed chopped-fiber materials, designated *B4*; and a 4-material bar composed of 1 continuous and 2 chopped fiber layers, as well as a small steel core (8mm diameter), designated *B5*. In the first chopped-fiber layer scheme (*B4*), two layers are composed of intermediate modulus carbon (IM-Carbon) chopped fibers and small modulus carbon chopped (SM-Carbon) fibers, respectively, while the two remaining layers are continuous aramid (Kevlar-49) and continuous E-glass fiber. Bar *B5* is similar but it has a steel rather than E-glass core. This further reduces costs, and at the core, the steel is protected from the environment by the outer layers, as suggested by Terry [9]. The chopped fiber composite layers consist of 65% resin and 35% fiber, while the fibers are taken as randomly dispersed with a fiber length of 6 mm.

The chopped-fiber layer schemes are considered due to an expected reduction in cost from using continuous fiber materials [16, 17]. Although less expensive than continuous fibers, a drawback is the strength and stiffness reduction associated with short fiber lengths and random dispersion. This is an important consideration for overall bar performance, particularly with regard to layer failure sequence. For the bar to behave in a ductile manner, when the first fiber type fails, the remaining layers must have the capacity to carry the applied load. Similarly, when the second fiber type fails, the remaining layers must still carry the load, and so on, until the last material fails when the desired ductility is reached. In the schemes presented, it is preferable that the carbon layers are placed on the exterior of the bar to protect the inner glass layers from alkaline attack in a cementitious environment.

Table 1 provides the volume fractions of the materials used in each bar, while Table 2 lists Young's modulus (E) and ultimate strain (ε_u) of these materials. Note that these configurations are not arbitrary, but carefully selected in order to meet both strength and ductility requirements, as described below.

BAR ANALYSIS

The elastic modulus of a composite material composed of continuous fibers loaded in tension can be estimated with the rule of mixtures:

$$E_c = E_m v_m + \sum_i E_{fi} v_{fi} \qquad (1)$$

where E_c is the tensile modulus of elasticity of the composite in the longitudinal direction; E_m is the matrix/resin elastic modulus; v_m is the volume fraction of the matrix/resin; E_{fi} is the fiber tensile elastic modulus for material i, and v_{fi} is the volume fraction of material i.   The corresponding tensile stress in the composite, σ_c can be similarly calculated by multiplying E_c with the composite strain ε_c. For the scheme with a steel core, stress in the bar is calculated as $\sigma_c = E_c \varepsilon_c + \sigma_y v_{steel}$ for strains beyond steel yield strain, where v_{steel} is steel volume fraction and σ_y steel yield stress. In this formulation, strain compatibility (i.e. perfect bond) is assumed to exist between the different materials in the HDFRP bars, such that the tension force can be fully transferred via shear from outer to inner materials. Based on the existing experimental data summarizing tension, pull-out, and flexural tests, in which no significant slip between material layers was reported, this appears to be a reasonable model [1, 9-15].

When chopped fiber layers are included in the composite bar, eq. (1) must be adjusted to account for the reduced effective modulus of the chopped fiber layers.   This can be done by

applying appropriate reduction factors to eq. (1), which takes into account the effects of fiber length and orientation:

$$E_c = \eta_{LE} \cdot \eta_{OE} \cdot E_f . v_f + E_m v_m \qquad (2)$$

where E_c is the modulus of elasticity of the composite in the longitudinal direction; E_f is the modulus of elasticity of continuous fiber; E_m is the modulus of elasticity of the matrix; η_{LE} is the fiber length efficiency factor; and η_{OE} is the fiber orientation efficiency factor. η_{LE} can be calculated from [18]:

$$\eta_{LE} = 1 - \frac{\tanh(\beta l/2)}{\beta l/2} \qquad (3)$$

where

$$\beta = \frac{1}{r_f}\sqrt{\frac{2G_m}{E_f \ln\left(\dfrac{R}{r_f}\right)}} = \sqrt{\frac{8G_m}{E_f D^2 \log_e\left(\dfrac{2R}{D}\right)}} \qquad (4)$$

In these expressions, l is the chopped fiber length; G_m is the shear modulus of the matrix; E_f is the fiber elastic modulus, r_f is the fiber radius; and D is the fiber diameter. 2R refers to the mean center-to-center distance between fibers, and can be calculated from: $\dfrac{R}{r_f} = \sqrt{\dfrac{K_R}{v_f}}$. The value of K_R depends on the fiber packing geometry. For square packing, as assumed in this study, $K_R = \pi/4$ [19] (Figure 2). Eq. (3) describes a reduction in effective fiber modulus E_f for using short, equal-length fibers in the matrix in place of continuous fibers; $E_{f\ short} = \eta_{LE}E_{f\ continuous}$. As given in [18], the expression was derived assuming $E_f \gg E_m$ and perfect fiber-matrix bond. Values of η_{LE} may range from 0.20-0.99 for $v_f = 0.3$ with fiber lengths from 0.1-10 mm and fiber diameters of 8-10 μm [20], with reasonable agreement to experimental results [21]. In this study,

chopped fibers are taken as a uniform length of 6 mm and diameter of 10 μm, and have a corresponding η_{LE} of approximately 0.98-0.99.

The fiber orientation efficiency factor η_{OE} accounts for effective modulus reductions based on fibers misaligned from the load axis; $E_{f\ misaligned} = \eta_{OE}E_{f\ aligned}$; for aligned chopped fibers, $\eta_{OE}=1$, whereas for fibers transverse to the load, neglecting the effect of transverse deformation, $\eta_{OE}= 0$. For fibers with arbitrary orientation, η_{OE} becomes [22]:

$$\eta_{OE} = \sum_n a_n \cos^4 \phi_n \qquad (5)$$

where a_n is the fraction of fibers with orientation angle ϕ_n with respect to the load axis. Randomly-dispersed, in-plane fibers, as considered in this study, have been modeled using eq. (5) assuming fibers are equally divided into four representative orientations with 45° separation each (i.e. with ϕ_i = 0, 45, 90, and -45°, and a_i = ¼), resulting in $\eta_{OE} = \dfrac{3}{8}$ (note fibers randomly dispersed in three dimensions produces = 0.5) [22]. This result has shown good agreement with experimental data [23, 24].

The composite modulus of elasticity values predicted from eq. 2 has shown good agreement to the existing experimental data [24, 25]. For strength consideration, ultimate strength σ_{cu} of a chopped fiber layer can be calculated as:

$$\sigma_{cu} = \eta_{LS} \cdot \eta_{OS} \cdot \sigma_f \cdot v_f + \left(1 - v_f\right)\sigma_m, \qquad (6)$$

where η_{LS} is the fiber length efficiency factor for strength, calculated as $1 - \dfrac{l_c}{2l}$ for lengths greater than critical length l_c, and is 0.95 for the fibers used in this study [26]; η_{OS} is the fiber orientation efficiency factor, taken as 0.2 [27]; σ_f is fiber failure stress; σ_m is the matrix

stress at fiber failure strain, and v_f is the volume fraction of fiber in the layer. Chopped fiber length has a significant impact on stiffness, strength, and failure mode. The critical fiber length, l_c represents the minimum length that will allow tensile failure of the fiber rather than shear failure (i.e pull-out) at the interface, and is given in terms of fiber tensile stress σ_f, fiber diameter D, and the shear strength, τ, of the fiber-matrix interface or of the matrix itself (taken as 29 MPa in this study), whichever is lower, in the following expression: $l_c = \dfrac{\sigma_f D}{2\tau}$. Typical values for critical fiber length are 0.2 mm for carbon fibers embedded in epoxy resin, 0.5 mm for glass fibers in polyester resin, 1.8 mm for glass fibers in polypropylene resin [17]. Once the fiber length is 5 times the critical fiber length, approximately 90% of the fracture stress can be achieved. In this study, the chopped fiber length (6 mm) is taken as 8 times the critical fiber length.

DESIGN CONSTRAINTS

For HDFRP-reinforced concrete flexural members, in addition to strength, various other design constraints must be considered. Some of these include ductility, stiffness, bond, deterioration, and cost. In this work, it is assumed that the exterior fibers of the bar are sand-coated or otherwise appropriately ribbed for adequate bond [28, 29], while appropriate strength reduction factors to account for potential deterioration are given in *ACI 440.1R* in terms of the environmental factor C_E. Ductility and cost are more specifically addressed below.

For reinforced concrete flexural members that use composite materials as tension reinforcement, ductility index can be calculated from the load deflection or moment curvature diagram with the expression [30]:

$$\mu_\phi = \frac{1}{2}\left(\frac{E_{\text{total}}}{E_{\text{elastic}}} + 1\right) \tag{7}$$

where E_{total} is computed as the area under the load displacement or moment curvature diagram and E_{elastic} is the area corresponding to the elastic deformation. In this study, a minimum ductility index of 3.0 is specified for flexural member performance, which represents a lower limit similar to that of many steel-reinforced sections [31, 32].

As discussed previously, HDFRP bar ductility is generated from non-simultaneous material failures, such that after a material fails, the remaining materials have the capacity to carry the tension force until the final material fails, to produce the desired ductility level. Correspondingly, before the desired level of ductility is reached, each bar material must fail before the concrete crushes in compression, which is assumed to occur at an ultimate strain of $\varepsilon_{cu} = 0.003$. Enforcing the first constraint results in a bar stress-strain diagram that has subsequent stress peaks that do not decrease as bar strain increases, as shown in Figure 3 for bars *B1-B5*.

To evaluate the ductility of a HDFRP-reinforced section, the load deflection or moment-curvature function is needed. In this study, the latter is considered. Prior to concrete cracking, moment capacity M is calculated from elastic section properties according to $M = \frac{f_r I_g}{y_t}$, where f_r is the modulus of rupture of the concrete, I_g is the uncracked section moment of inertia, and y_t is the distance from the centroid of the section to the extreme tension fiber. The concrete stress-strain behavior for cracked sections is developed based on the modified Hognestad model [33], and the corresponding resisting moment is then determined from: $M = C_c(d - K_2 c)$, where C_c is the compressive force in the concrete; d is the distance from the top of the concrete compression

block to the reinforcement centroid; and c is the distance from the top of the concrete compression block to the section neutral axis. To develop the moment-curvature response, curvature ϕ_c is calculated from $\phi_c = \dfrac{\varepsilon_c}{c}$, where ε_c is the concrete strain at the top of the concrete compression block. For development of the moment-curvature diagram, it is assumed that once the failure strain of a particular bar layer is reached, the layer throughout the length of the bar immediately loses all force carrying capability. This conservative assumption results in the non-smooth moment-curvature diagrams shown in Figure 4. At the peak moment values on the diagrams, two different capacity values are theoretically associated with the same curvature. This occurs because once the stiffest existing material in the bar fails, the stiffness of the cracked section decreases and less moment is required to deform the beam the same amount. Experimental results of HDFRP-reinforced beams have developed somewhat smoother curves, closer to that found by drawing a line between the moment peaks and excluding the capacity drops as shown in Figure 4 [9, 12]. However, because including the theoretical low capacity points results in the most conservative ductility indices, this method is used to enforce the ductility constraint imposed in this study. Based on the material properties considered (Table 2), this results in sections with tension reinforcement strain ε_t significantly higher (approximately $0.02 < \varepsilon_t < 0.04$) at concrete crushing than that required by *ACI 318* for a tension controlled ($\phi = 0.9$) steel reinforced section ($\varepsilon_t \geq 0.005$). All of the bar configurations considered meet these ductility constraints.

The nominal moment capacity M_n of the HDFRP-reinforced concrete section is taken as the first peak on the moment-curvature diagram, which represents the moment at which the first FRP material (i.e. lowest ultimate strain) in the bar ruptures, which is IMCF-I for *B4* and *B5* and IMCF-II for *B1-B3* (see Tables 1 and 2).

For all bar schemes except *B5*, in which all materials are composed of fiber, ignoring the concrete tensile strength, which is insignificant in section flexural resistance, an expression of HDFRP-reinforced concrete moment capacity can be developed as:

$$M_c = \left[d - K_2 \frac{\varepsilon_{f_1}}{K_1 \cdot f_c' \cdot b} \left(\sum_{i=1}^{n} v_{f_i} E_{f_i} + v_m E_m \right) \left(\sum_{i=1}^{n} v_{f_i} + v_m \right) A_T \right] \cdot$$

$$\left[\varepsilon_{f_1} \left(\sum_{i=1}^{n} v_{f_i} E_{f_i} + v_{f_m} E_{f_m} \right) \left(\sum_{i=1}^{n} v_{f_i} + v_m \right) A_T \right] \tag{8}$$

The first square bracketed term represents the distance between the centroids of the concrete compressive block and the reinforcement, while the second square bracketed term is the force in the reinforcement at first bar material failure.   In eq. (8), K_1 and K_2 are parameters used to define the parabolic shape of the concrete compression block in Hognestad's nonlinear stress-strain model, where K_1 represents the ratio of the average concrete stress to the maximum stress f_c' in the compressive block, while K_2 provides the location of the centroid of the compressive block, in terms of a fraction of the neutral axis depth, as measured from the extreme fiber in compression; A_T is the total area of reinforcement; d is the distance from the tension reinforcement centroid to the extreme compression fiber in the beam; and b is the width of the concrete compression block, as shown in Figure 5.   For scheme *B5*, with a steel core, the resistance moment can be developed as:

$$M_c = \left[d - K_2 \frac{\left(\sum_{i=1}^{n} v_{f_i} + v_s + v_m \right) A_T}{K_1 \cdot f_c' \cdot b} \left\{ \left(\sum_{i=1}^{n} v_{f_i} E_{f_i} + v_m E_m \right) \varepsilon_{f_1} + v_s \cdot f_y \right\} \right] \cdot$$

$$K_1 \cdot f_c' \cdot b \left[\frac{\left(\sum_{i=1}^{n} v_{f_i} + v_s + v_m \right) A_T}{K_1 \cdot f_c' \cdot b} \left\{ \left(\sum_{i=1}^{n} v_{f_i} E_{f_i} + v_m E_m \right) \varepsilon_{f_1} + v_s \cdot f_y \right\} \right] \tag{9}$$

where the second bracketed term represents the compressive force in the concrete at first material failure; v_s is the volume fraction of steel; and f_y is the yield stress of steel. Note for bars *B4* and *B5*, where chopped fiber layers are considered, the effective elastic modulus of the chopped fibers E_{fi} is calculated as $E_{fi} = \eta_{LE} \cdot \eta_{OE} \cdot E_f . v_f$,

Due to the lower effective modulus of many composite materials as compared to steel, and particularly for chopped fiber layers, the possibility of excessive deflections must be considered. This concern is recognized in *ACI 440.1R*, where recommended limits on span/depth ratios for composite-reinforced concrete flexural members are given. The estimation of flexural deflections in reinforced-concrete members becomes challenging, since the degree of cracking, and corresponding loss of stiffness, generally varies along the length of the flexural member. To account for this, various methods are available, one of which is presented by Branson [34, 35], which estimates the effective moment of inertia I_e as:

$$I_e = \left(\frac{M_{cr}}{M_a} \right)^3 \beta_d I_g + \left[1 - \left(\frac{M_{cr}}{M_a} \right)^3 \right] I_{cr} \leq I_g \tag{10}$$

where M_{cr} is the cracking moment and M_a is the applied moment. Although the general form of the above equation was developed for steel-reinforced sections, an additional reduction factor, β_d, is used to account for the typical lower stiffness associated with FRP reinforcing and potential bonding problems. To estimate deflections in this study, β_d is calculated as $\beta_d = 3.3 \frac{I_{cr}}{I_g}$, where I_g and I_{cr} are gross and cracked moment of inertias, respectively [36].

EVALUATION CASES

Two typical tension-controlled reinforced concrete flexural member applications are considered; a bridge deck and a building floor beam. For the bridge deck (Figure 6), three girder spacings are considered; 1.8, 2.7, and 3 m (6, 9, and 10 ft), with corresponding slab thicknesses of 180, 200, and 230 mm (7, 8, and 9 in), with a 13 mm (0.5 in) integrated wearing surface and a 65 mm (2.5 in) future wearing surface allowance. Concrete strength is taken as f_c'= 31 MPa (4500 psi), while 22 mm (7/8 in) diameter HDFRP bars are placed in the top and bottom of the slab with 25 mm (1 in) cover, as constructed in two FRP-reinforced bridge decks built in Wisconsin [29, 37]. For reference, *AASHTO GFRP* [8] specifies a minimum of 19 mm (¾ in) cover for slabs reinforced with FRP bars. To allow use of HDFRP ductility, the deck is designed as a tension-controlled member for positive and negative moments using the equivalent strip method according to *AASHTO LRFD* [5], where the governing design equation is:

$\phi M_n = \gamma_{DC} M_{DC} + \gamma_{DW} M_{DW} + 1.75 M_{LL+IM}$. Here, ϕ is taken as 0.55 [8]; M_{DC} and M_{DW} are moments caused by the self weight of the deck and wearing surface, respectively; γ_{DC} are γ_{DW} are load factors that may vary from 1.25 to 0.9, and 1.5 to 0.65, respectively, to generate maximum load effect; and M_{LL+IM} is the moment caused by 72 kN (16 kip) truck wheel loads on the slab (in addition an impact factor of 1.33), positioned to generate greatest moment. An environmental factor used to account for material degradation is taken as C_{E} = 0.9, as recommended in *ACI 440.1R* for carbon FRP bars, as in this study, the outer material of the HDFRP bars considered are carbon. A summary of the resulting deck slab reinforcement ratios (ρ), ductility indices (μ_ϕ), and maximum deflections (Δ, mm) are given in Table 3. As shown, reinforcement ratios were approximately 0.002-0.006. The resulting ductility indices ranged from approximately 3 for slabs

reinforced with bars *B1-B2*, 4 - 5 for bar *B5*, 5 - 6 for bar *B3*, and 6 – 7 for bar *B4*. Note that these values are higher than the steel-reinforced slabs. This is because the post 'yield' (i.e. after first material failure) deformations of HDFRP-reinforced slabs are greater than those of the corresponding steel reinforced sections before ultimate failure (concrete crushing). Deflections were similar for all HDFRP-reinforced schemes, and approximately twice that of steel-reinforced slabs of the same depth, as shown in Table 3.

For the building beam (Figure 7), three span lengths, 6, 7.6, and 9.1 m (20, 25, and 30 ft), were considered, with f_c' = 38 MPa (5500 psi). A simple-span beam was considered for analysis, although a continuous member does not significantly alter results. The beam width was 300 mm (12 in). Beam height was selected to satisfy the minimum recommendation given in *ACI-440.1R* for non-prestressed FRP-reinforced beams (1/10 of span length for simply supported beams), which resulted in reinforcement depths *d* of 560 mm (22 in) for the 6 m span, 710 mm (28 in) for the 7.6 m span, and 865 mm (34 in) for the 9.1 m span. As with the slab, a tension-controlled member is considered. The relevant flexural design equation is $\phi M_n = 1.2 M_{DL} + 1.6 M_{LL}$, where ϕ is 0.55 [7] and M_{DL} and M_{LL} are the dead and live load moments, respectively. Resulting beam characteristics are presented in Table 4. Also included for comparison are a steel-reinforced beam of the same dimensions as the FRP-reinforced section and a steel-reinforced beam using the span/depth recommendation given in *ACI 318* (1/16 of span length for simple beams for simple spans), resulting in *d* = 318 mm (12.5 in), 412 mm (16.3 in), and 510 mm (20 in) for the 6, 7.6, and 9.1 m spans, respectively. As shown, HDFRP reinforcement ratios were from 0.003-0.01. Ductility indices ranged from approximately 3.3 – 3.4 for beams reinforced with bars *B1* and *B2*, and from approximately 5 - 6 when reinforced with bars *B3, B4*, and *B5*. Steel-reinforced beam ductility indices were 3 for the smaller *ACI-318*

span/depth ratio beams and 7 for the deeper beams matching the HDFRP-reinforced section dimensions. Deflections were similar for all HDFRP-reinforced schemes, where, similar to the bridge slab results, steel-reinforced section deflections were about half that of the HDFRP sections of the same depth. Using the larger span/depth ratios recommended in *ACI-318* for the steel-reinforced sections (case "Steel 2" in Table 4) produced deflections approximately equal to the thicker-deck HDFRP sections.

It should be noted that to date, experimental results have considered determinate members, and the effect of the pseudo-ductile response of HDFRP-reinforced members on load redistribution during overloads has not been studied. This is an area of potential concern and additional research is needed to verify performance in structural systems.

COST COMPARISON

Although various factors affect cost, two primary considerations include material and manufacturing costs. For comparing material costs, in this study, specific cost *sc*, as a proportion of HDFRP bar cost to that of steel, is considered:

$$sc = \frac{C_f \, \rho_f}{C_s \, \rho_s} \tag{11}$$

where C_f is the cost of fiber material per unit weight, ρ_f is the density of the fiber, C_s is the cost of steel, and ρ_f is steel density. The specific costs considered in this study are given in Table 2, as taken from the available literature [9, 16, 28]. During the material manufacturing process, chopped fibers generally need not be dried or wound onto bobbins as with continuous fibers, resulting in a potentially significant cost reduction, estimated to be 1:1.6 for chopped fiber layers as compared to continuous fibers [16]. The resulting relative unit costs per weight of the bar

schemes is given in Table 5, which indicates that bars using chopped fiber layers (*B4, B5*) are least expensive. However, bars using chopped fiber layers require more overall material to account for losses in strength as compared to continuous fibers. The total relative cost of using each bar is also given in Table 5, which is found by multiplying the relative unit cost by the average reinforcement ratio for the example applications considered. In this case, the least expensive schemes are composed entirely of continuous fiber layers (*B1-B3*). Of these, the bars composed of 3 and 4 materials are least expensive overall (*B2, B3*). Note that Terry [9] proposed a continuous ductile bar scheme which is in fact significantly less expensive than all bars presented in Table 5. However, the cost savings results from the fact that the bar is largely steel (60%; as compared to 20% for *B5* in this study), which may limit its long-term durability in a corrosive environment.

As HDFRP bars have yet to be mass-produced on a wide scale for commercial sale, there is no readily available product manufacturing data to compare other cost influences. Thus, the values given in Table 5 are initial estimates only.

CONCLUSIONS

With careful selection of bar material properties and proportions, all HDFRP-reinforced flexural members considered could meet code-specified strength and ductility requirements for steel-reinforced sections, though service load deflections were approximately twice that of steel-reinforced sections of the same depth. As it was found that HDFRP-reinforced sections using the span/depth ratios recommended in *ACI-440.1R* were similar to steel-reinforced sections using the span/depth ratios given in *ACI-318*, the existing *ACI-440.1R* recommendations appear to well-apply to sections reinforced with HDFRP bars as well. With the range of material choices

considered in this study, sections reinforced with continuous fiber HDFRP bars (*B1-B3*) required lower reinforcement ratios than beams reinforced with Grade 60 steel, though sections using chopped fiber layer bars (*B4, B5*) required approximately twice the reinforcement ratio of the continuous fiber bars to meet strength requirements.   The chopped fiber layer schemes were less expensive per bar, but more costly overall than continuous bars. Continuous fiber bars with 2 and 3 materials (*B1, B2*) had ductility indices slightly greater than 3, the lower limit of acceptability in this study, while when 4 materials were considered (*B3*), ductility index increased to approximately 5. The 4 material chopped fiber bar had greatest ductility, from 6-7, equivalent to the same section with steel reinforcing.

Although the chopped fiber layer bars provided greatest ductility, the associated large reductions in strength, and corresponding need for larger reinforcement ratios, resulted in this bar type as a relatively costly option.   For the continuous fiber bars, ductility increased, and material costs decreased, as layers increased from 2 to 4. This resulted in the 4-material continuous fiber bar approach to be most promising, with high ductility as well as relatively low cost.

REFERENCES

1. Won, J-P, Park, C-G, and Jang, C-I. (2007). "Tensile Facture and Bond Properties of Ductile Hybrid FRP Reinforcing Bars." Polymers & Polymer Composites 15(1): 9-16.

2. FHWA. (2001). "Long Term Effectiveness of Cathodic Protection Systems on Highway Structures." Publication No. FHWA-RD-01-096. McLean, VA: Federal Highway Administration.

3. Smith, J.L. and Virmani, P.Y. (1996). "Performance of Epoxy-Coated Rebars in Bridge Decks." Public Roads 60(2).

4. Eamon, C., Jensen, E., Grace, N., and Shi, X. (2012). "Life Cycle Cost Analysis of Alternative Bridge Reinforcement Materials for Bridge Superstructures Considering Cost and Maintenance Uncertainties." ASCE Journal of Materials in Civil Engineering. 4(24): 373-380.

5. AASHTO LRFD Bridge Design Specifications, 5th ed. (2010). Washington, D.C.: American Association of State and Highway Transportation Officials.

6. ACI 318-11: Building Code Requirements for Structural Concrete and Commentary. (2011) Farmington Hills, MI: American Concrete Institute.

7. ACI 440.1R-06: Guide for the Design and Construction of Structural Concrete Reinforced with FRP Bars. (2006). Farmington Hills, MI: American Concrete Institute.

8. AASHTO LRFD Bridge Design Guide Specifications for GRFP-Reinforced Concrete Bridge Decks and Traffic Railings. (2009). Washington, D.C.: American Association of State and Highway Transportation Officials.

9. Terry, K.C. (2006). "Behavior of Concrete beams reinforced with Hybrid FRP composite Rebars." MS Thesis, Hong Kong University of Science and Technology, Dept. of Civil Engineering, September.

10. Belarbi, A., Watkins, S.E., Chandrashekhara, K., Corra, J., and Konz, B. (2001). "Smart fiber-reinforced polymer rods featuring improved ductility and health monitoring capabilities." Smart Materials and Structures 10: 427-431.

11. Tamuzs, V. and Tepfers, R. (1995). "Ductility of non-metallic hybrid fiber composite reinforcement for concrete." Proceedings of the Second International RILEM Symposium, Ghent, Belgium. August.

12. Harris, H.H., Somboonsong, W., and Ko, Frank K. (1998). "New Ductile Hybrid FRP Reinforcing Bar for Concrete Structures." ASCE Journal of Composites for Construction 2(1): 28-36.

13. Bakis, E.C., Nanni, A., and Terosky, J.A. (2001). "Self-monitoring, pseudo-ductile, hybrid FRP reinforcement rods for concrete applications." Composite Science Technology 61: 815-823.

14. Cui, Y-H and Tao, J. (2009). "A new type of ductile composite reinforcing bar with high tensile elastic modulus for use in reinforced concrete structures." Canadian Journal of Civil Engineering 36: 672-675.

15. Wierschem, N. and Andrawes, B. (2010). "Superelastic SMA-FRP composite reinforcement for concrete structures." Smart Materials and Structures 19.

16. Janney, M., Geiger, E., and Baitcher, N. (2007). "Fabrication of Chopped Fiber Preforms by the 3-DEP Process." Composites & Polycon. American Composites Manufacturers Association.

17. Matthews, F.L., and Rawlings, R.D. (1999). "Composite Materials: Engineering and Science." CRC Press.

18. Cox, H.L. (1952). 'The Elasticity and Strength of Paper and Other Fibrous Materials." British Journal of Applied Physics 3(3): 72-79.

19. Pan, M., (1993). "Theoretical Determination of The Optimal Volume Fraction and Fiber-Matrix Property Compatibility of Short Fiber Composites." Polymer Composites 14(2): 85-93.

20. Hull, D. (1981). "An Introduction to Composite Materials." Cambridge University Press.

21. Dingle, L.E. (1974). "Aligned Discontinuous Carbon Fiber Composites." Proceedings, 4th International Conference on Carbon Fibers, Their Composites and Applications. Plastic Institutes, London.

22. Krenchel, H. (1964). "Fiber Reinforcement." Akademisk Forlag, Copenhagen.

23. Manera, M. (1977). "Elastic Properties of Randomly Oriented Short Fiber-Glass Composites." Journal of Composite Materials, 11: 235-247.

24. Fu, S.Y., and Lauke, B. (1998). "The Elastic Modulus of Misaligned Short-Fiber-Reinforced Polymers." Composites Science and Technology, 58(3-4): 389-400.

25. Andersons, J., Joffe, R., and Sparnins, E. (2006). "Stiffness and Strength of Flax Fiber/Polymer Matrix Composites." Polymer Composites 27(2): 221-229.

26. Behnam, B.R. (2012) "Reliability Model for Ductile Hybrid FRP Rebar Using Randomly Dispersed Chopped Fibers." PhD Dissertation, Wayne State University, Dept. of Civil and Environmental Engineering, May.

27. Thomason, J.L., Vlug, M.A., Schipper, G., and Kirkor, H.G.L.T., (1996). "Influence of Fiber Length and Concentration on the Properties of Glass-Fiber Polypropylene: Part 3. Strength and Strain at Failure." Composites Part A: Applied Science and Manufacturing, 27(11):1075-1084.

28. Bank, L.C. (2006). Composites for Construction Structural Design with FRP Materials." Wiley.

29. Bank, L.C., Oliva, M.G., Russell, J.S., Jacobson, D.A., Conachen, M, Nelson, B, and McMonigal, D. (2006). "Double-Layer Prefabricated FRP Grids for Rapid Bridge Deck Construction: Case Study." Journal Of Composites For Construction 10(3): 204-212.

30. Naaman, A. E., and Jeong, S. M., (1995). "Structural Ductility of Concrete Beams Prestressed with FRP Tendons." Proceedings of the Second International RILEM Symposium, Ghent, Belgium, August.

31. Maghsoudia, A.A., and Bengarb, H.A., (2011). "Acceptable Lower Bound of The Ductility Index and Serviceability State of RC Continuous Beams Strengthened with CFRP Sheets." Scientia Iranica 18: 36–44.

32. Shin, S., Kang, H., Ahn, J., and Kim, D. (2010). "Flexural Capacity of Singly Reinforced Beam with 150 MPa Ultra High-Strength Concrete." Indian Journal of Engineering & Materials Science 17: 414-426.

33. Hognestad, E. (1952). "Inelastic Behavior in Tests of Eccentrically Loaded Short Reinforced Concrete Columns," ACI Journal Proceedings, 24(2): 117-139.

34. Branson, D.E. (1977). "Deformation of Concrete Structures." New York, McGraw-Hill.

35. Branson, D.E. (1965). "Instantaneous and Time-Dependant Deflections of Simple and Continuous Reinforced Concrete Beams." HPR Report No. 7, Part 1, Alabama Highway Department, Bureau of Public Roads, Auburn, AL: Department of Civil Engineering and Auburn Research Foundation, Auburn University.

36. Bischoff, P. H. (2007). "Deflection Calculation of FRP Reinforced Concrete Beams Based on Modifications to the Existing Branson Equation." Journal of Composites for Construction, ASCE, 11(1).

37. Berg, A.C., Bank, L.C., Oliva, M.G., Russell, J.S. (2006). "Construction and cost analysis of an FRP reinforced concrete bridge deck." Construction and Building Materials 20(8): 515–526.

Table 1. Material Volume Fractions in Considered HDFRP Bars

Bar Number:	B1	B2	B3	B4	B5
No. of Layers:	2	3	4	4	4
IMCF-I*	-	-	-	0.19	0.15
IMCF- II	0.29	0.20	0.20	-	-
SMCF-I	-	0.06	0.07	-	-
SMCF-II*	-	-	-	0.09	0.06
AKF-I	-	-	-	0.04	0.10
AKF-II	0.29	0.25	0.10	-	-
EGF	-	-	0.17	0.06	-
Steel	-	-	-	-	0.20
Resin	0.42	0.49	0.46	0.62	0.49

*Chopped fiber layers

Table 2. HDFRP Bar Material Properties

Label	Material	E GPa (ksi)	ε_u	Density (g/cc)	Specific cost
IMCF-I	IM-Carbon Fiber Type I	650 (95000)	0.0045	1.76	70
IMCF-II	IM-Carbon Fiber Type II	400 (58000)	0.0050	1.76	50
SMCF-I	SM-Carbon Fiber Type I	238 (34500)	0.0150	1.76	6.0
SMCF-II	SM-Carbon Fiber Type II	230 (33400)	0.0150	1.76	6.0
AKF-I	Aramid Kevlar-49 Fiber Type I	125 (18000)	0.0250	1.45	8.0
AKF-II	Aramid Kevlar-49 Fiber Type II	102 (15000)	0.0250	1.45	8.0
EGF	E-Glass fiber	74 (11000)	0.0440	2.56	1.0
Steel	Steel, Grade 60	200 (29000)	0.0207	7.80	1.0
Resin	Epoxy	3.5 (540)*	0.0600	1.05	1.5

*Shear modulus G is taken as 1.26 MPa (194 ksi). Note yield stress for steel is given.

Table 3. Bridge Deck Characteristics

	Bridge Deck Reinforcement					
	B1	B2	B3	B4	B5	Steel
L=1.8 m (6 ft), h= 180 mm (7 in)						
ρ	0.0026	0.0031	0.0032	0.0066	0.0061	0.0046
μ_ϕ	3.3	3.2	5.2	6.4	4.3	3.0
Δ	10.1	10.0	10.0	9.2	9.1	4.8
L=2.7 m (9 ft), h = 200 mm (8 in)						
ρ	0.0025	0.0030	0.0031	0.0064	0.0059	0.0044
μ_ϕ	3.2	3.4	5.5	6.8	4.8	3.0
Δ	20.2	20.3	20.1	18.0	17.9	9.5
L=3.0 m (10 ft), h = 230 mm (9 in)						
ρ	0.0023	0.0028	0.0028	0.0060	0.0056	0.0041
μ_ϕ	3.3	3.3	5.8	6.8	5.0	3.0
Δ	18.0	18.1	18.1	16.2	16.0	8.7

Table 4. Beam Characteristics

	Beam Reinforcement						
	B1	*B2*	*B3*	*B4*	*B5*	Steel	Steel 2*
L=6 m (20 ft)							
ρ	0.0040	0.0048	0.0049	0.0102	0.0094	0.0073	0.020
μ_ϕ	3.3	3.4	5.2	6.3	4.6	7.0	3.0
Δ	29.7	29.7	29.7	27.2	27.2	14.2	33.3
L=7.6 m (25 ft)							
ρ	0.0038	0.0046	0.0046	0.0097	0.0090	0.0069	0.019
μ_ϕ	3.3	3.4	5.2	6.6	5.0	7.0	3.0
Δ	36.6	36.3	36.3	32.8	32.8	17.3	38.4
L=9.1 m (30 ft)							
ρ	0.0032	0.0039	0.0039	0.0083	0.0077	0.0064	0.0172
μ_ϕ	3.3	3.3	5.2	6.6	5.0	7.0	3.0
Δ	41.4	41.4	41.7	37.7	37.8	19.9	43.7

*Span/depth recommendation as per ACI-318.

Table 5. HDFRP Bar Relative Cost

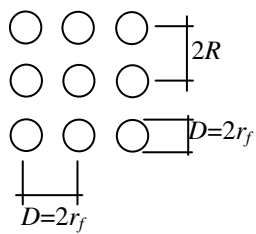| Bar	Relative Unit Cost	Relative Total Cost
B1	1.96	1.26
B2	1.29	1.00
B3	1.29	1.01
B4	1.14	1.88
B5	1.00	1.53
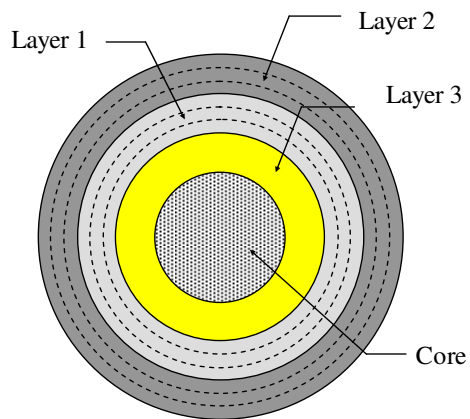
Figure 1. HDFRP Bar Concept

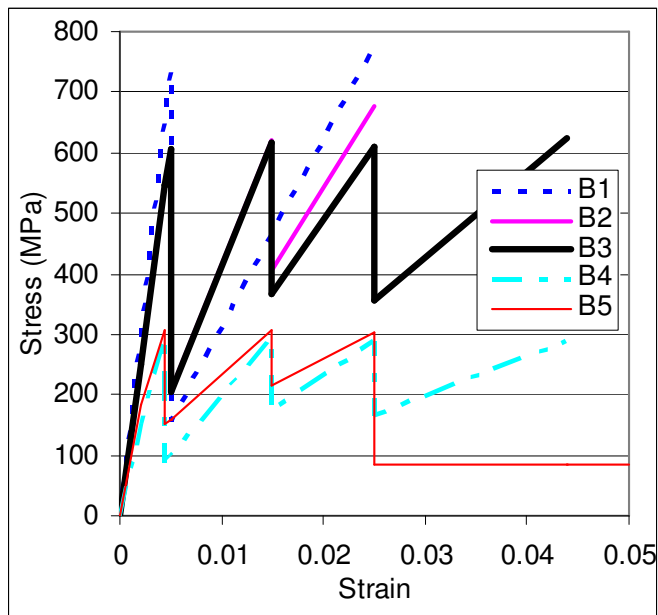**Figure 2. Square Packing Arrangement**

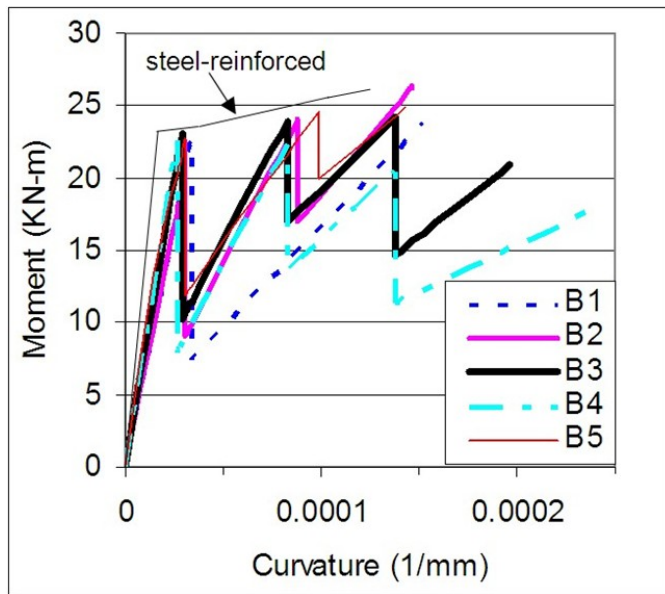**Figure 3. Stress-Strain Curves for HDFRP Bars**

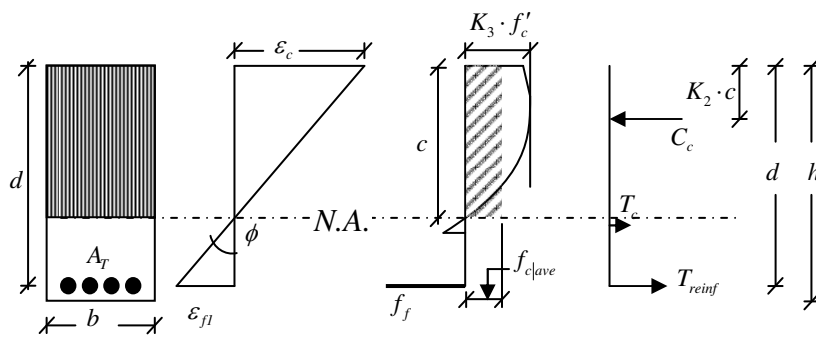**Figure 4. Moment-Curvature Diagram of HDFRP-Reinforced Beams**

Figure 5. Beam Section

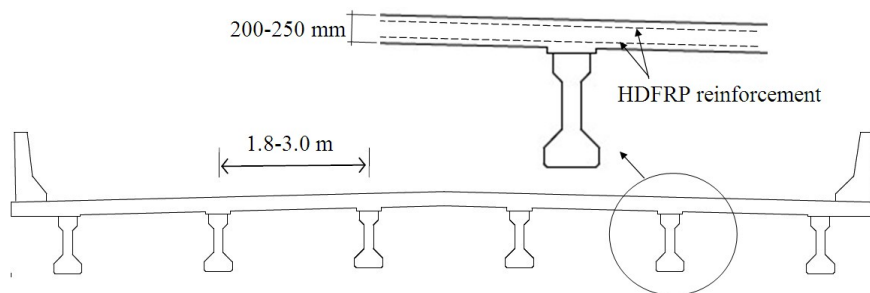**Figure 6. Bridge Deck**

405-510 mm

600-910 mm

HDFRP
reinforcement

Figure 7. Building Beam